Lasing frequencies and thresholds of the dipole supermodes in an active microdisk concentrically coupled with a passive microring

Elena I. Smotrova,[1,*] Trevor M. Benson,[2] Phillip Sewell,[2] Jiri Ctyroky,[3] and Alexander I. Nosich[1]

[1]*Institute of Radio-Physics and Electronics, National Academy of Sciences of Ukraine, Kharkov 61085, Ukraine*
[2]*George Green Institute for Electromagnetics Research,University of Nottingham], Nottingham NG7 2RD, UK*
[3]*Institute of Photonics and Electronics, Academy of Sciences of the Czech Republic, v.v.i., 182 51 Prague 8, Czech Republic*
**Corresponding author: elena_smotrova@yahoo.com*

Received April 29, 2008; revised September 8, 2008; accepted September 17, 2008;
posted September 22, 2008 (Doc. ID 95577); published October 31, 2008

The lasing spectra and threshold values of material gain for the dipole-type supermodes of an active microdisk concentrically coupled with an external passive microring are investigated. TE polarized modes are treated accurately using the linear electromagnetic formalism of the 2-D lasing eigenvalue problem (LEP) with exact boundary and radiation conditions. The influence of the microring on the lasing frequencies and thresholds is studied numerically, demonstrating threshold reduction opportunities. This is explained through the analysis of the mode near-field patterns and the degree of their overlap with the active region, as suggested by the optical theorem applied to the LEP solutions. © 2008 Optical Society of America

OCIS codes: 140.0140, 140.3560, 140.3945, 140.3410.

1. INTRODUCTION

Microcavity lasers are expected to serve as key elements of compact photonic integrated circuits because of their small size and low-threshold operation. The lowest thresholds are observed in on-pedestal circular disks and in low-index-substrate cavities equipped with embedded quantum wells or layers of quantum dots. This is because such lasers work in the whispering-gallery (WG) modes whose optical fields experience almost total internal reflection at the disk rim [1–3]. To achieve a pronounced WG effect, the disk rim, being as smooth as possible, must be at least several wavelengths in the disk material, hence the angular index m of the working mode is usually not smaller than 5. Reduction of the microdisk size beyond this limit is desirable; however, it leads to an increase of the lasing threshold as the low-angular-index modes in subwavelength circular cavities do not display WG behavior [4]. Note also that in thin microdisks the modes form two distinctive families, one having the optical field with the H_z component dominating over the E_z component, and the other vice versa (the z axis being the disk axis). It is the former family, usually denoted as TE, that has smaller thresholds, as supported by numerous experiments. This has been convincingly explained with the aid of the effective refractive index theory: this quantity is always larger for the TE family of modes than for the TM one.

Apart from cascading several quantum wells in the stand-alone disk, there are two ways to lower the material threshold for the disk modes by modifying the disk environment. One is to collect several microdisks in a cyclic photonic molecule (CPM) [5,6]. Simulations show that because of the symmetry- or antisymmetry-assisted optical field interference, the Q factor of any specific optically coupled mode ("supermode") in the passive (pump off) CPM can be made larger [7], and the threshold in the active (pump on) CPM can be made lower than for a stand-alone cavity [8–10]. Here, working with small-m non-WG modes in each disk has an additional advantage. According to the modeling results the lowering of the threshold of a supermode built on the larger-m WG modes in elementary disks requires a very precise selection of the distance between adjacent disks [9]. This therefore requires either accurate prefabrication modeling or postfabrication geometry tuning, which is difficult to achieve. In contrast, for the supermodes built on the small-m TE-type non-WG modes, such as the $H_{0,1}$ or $H_{1,1}$ ones in each subwavelength elementary disk, the lowering of the thresholds can be achieved more easily by bringing them together in a very tight circular array [10]. In this case there are two convenient engineering tools: the number of elementary small-size cavities and the separation between them. The larger the number of cavities and the smaller the separation, the smaller the CPM threshold. Note that these effects, although predicted at the early stage of research [5] and now supported by simulations, still await experimental verification.

Another way to lower the threshold for a small subwavelength circular microdisk is to embed it into an annular Bragg reflector (ABR), which can provide in-plane radial optical confinement as a result of in-phase reflections [11,12]. Here, the number of pairs of ABR layers is usually exploited as an engineering design tool. In the on-substrate patterned designs with shallow grooves, it is frequent for experimental papers to display microphotographs of cavities placed inside ABRs of 30–100 periods.

In the case of deeply etched grooves this number can be made smaller due to the larger effective-index contrast between the layers, in the same manner as for the flat-layered Bragg reflectors [13].

Until recently the analysis of ABR-assisted circular cavities has been restricted to the study of *passive* resonators and the associated Q factors of their eigenmodes—see the comprehensive list of relevant publications in [14]. It is important to remember that the natural modes of any open cavity are discrete in the sense that their frequencies form a discrete set of numbers, always complex-valued. Mathematically, the modal Q factor is a quantity "rigidly" linked to a mode, i.e., it may also take only discrete values. Neglecting this fact is not unusual (see, e.g., [14]); however it leads to erroneous conclusions. For instance, it suggests plotting the Q factor as a continuous function of the real-valued frequency.

Analysis of the lasing thresholds for an ABR-assisted active cavity—i.e., a true microlaser—by using the balance between radiation losses and material optical gain is a different type of electromagnetic field problem. An attempt to consider an ABR laser of that type was reported in [15]; however, there the reduction from a 3-D to a 2-D model involved field functions that did not satisfy the Helmholtz equations, the size of active region was not specified, and the material gain was not considered as an eigenvalue. This analysis was greatly improved in [16], where the TE-type 2-D eigenvalue problem for the ABR laser was correctly considered with frequency and material threshold gain as eigenvalue parameters. Still the size of the active region, where the gain was assumed as an "active" imaginary part of the refractive index, was not clearly introduced, so that formally the whole infinite external domain was active. This is not true, of course, as experimental ABR lasers, even if etched out of one large sample with a quantum well stretching across the whole structure, always have a finite active region defined by the spot of the focused pumping beam [11]. Furthermore we note that using only one angular index m is not sufficient for identifying the lasing modes because each azimuth family contains an infinite number of modes, and the radial-dependence index (or indices) is (are) needed to remove the ambiguity.

Unlike the papers mentioned, here we will study in the 2-D approximation an active microdisk placed in the center of one passive microring and find the effect of the latter on the thresholds of the lasing modes of the "dipole" type, i.e., those having $m=1$. This model corresponds to the realistic situation when the pumping is applied to the central disk only, and the external circular layers remain passive. In computations, we will also assume that both the disk and the ring materials differ only in the presence or absence of material gain, respectively. The space between them is assumed to be filled with a passive material having a smaller refractive index; to emphasize the observed effects we will take it as air in computations. This situation models deeply etched, surface-relief, on-substrate ABR lasers and is also applicable to cylindrical capillary lasers [17]. Interestingly, in view of the recently reported achievement of fabrication of a 600 nm diameter disk laser standing on a 100 nm diameter pedestal [18], one may imagine that in principle a ring on a pedestal of similar width can be manufactured as well. We restrict our consideration to the TE-polarized modes and treat them accurately using the so-called LEP formalism whose details can be found in [4] (see also [3] and references therein).

In Section 2, we briefly review the formulation of LEP and the derivation of basic equations. Section 3 presents the numerical results demonstrating that any lasing mode is always a "supermode" because of the optical coupling between passive and active parts of the whole cavity. In Section 4, we show that the dependences of the mode thresholds on the geometrical and material parameters of the partial domains can be conveniently explained using the overlap coefficients suggested by the optical theorem. This analysis is presented in Section 5. In particular, the modal field of any disk mode can be pulled into the passive region (i.e., pushed out of the active region) leading to increased threshold. Conclusions are summarized in Section 6.

2. FORMULATION OF LASING PROBLEM AND BASIC EQUATIONS

The ABR-assisted microdisk laser is an example of an optical circuit consisting of several optically coupled elements, where the active region does not coincide with the whole resonance structure. This is because, as mentioned, ABRs are manufactured with multiple rings and grooves while the pumping beam is focused on the central cavity into a spot several micrometers in diameter to prevent the device from lasing on the ring modes. In this paper we study the simplest configuration of this sort, a uniformly pumped active disk inside one passive ring, with the space between them filled with a less optically dense material.

Figure 1 shows the in-plane geometry of a microdisk cavity placed in the center of a microring. We introduce the polar coordinates (r,φ) and denote the disk radius a, the separation between the disk and the ring d, and the thickness of the ring w. We assume that in the pump-off regime the disk has real-valued refractive index α_a. However, if the pumping is applied the disk becomes active and attains a uniform material gain γ, so that its refrac-

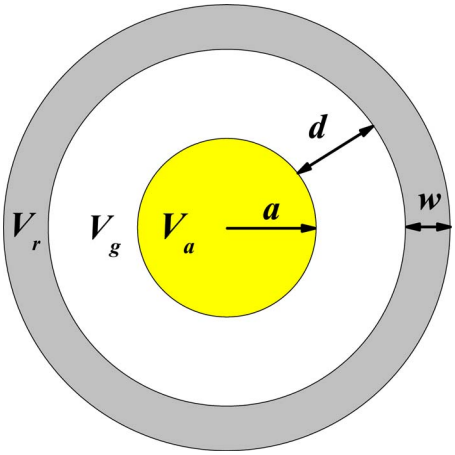

Fig. 1. (Color online) In-plane geometry of active circular microcavity concentrically coupled with a passive ring.

tive index becomes complex-valued: $v=\alpha_a-i\gamma$, $\gamma>0$. Here, the contribution of the pumping to the real part of the refractive index can be neglected as it is very small in comparison with α_a. The refractive index of the domain between the cavity and the ring is denoted α_g and the ring refractive index is α_r (for simplicity, both these refractive indices are assumed real-valued), and the outer medium is air. The time dependence is implied as $e^{-i\omega t}$, and the free-space wavenumber is $k=\omega/c=2\pi/\lambda$, where λ is wavelength.

In the 2-D model, we consider the TE polarization with the aid of the H_z field component denoted as $U(r,\varphi)$. The LEP statement implies that U must satisfy the Helmholtz equation with the piecewise constant coefficient equal to k^2, $k^2\alpha_r^2$, $k^2\alpha_g^2$, and k^2v^2 in the air, ring, gap, and active region, respectively. At all the boundaries, the continuity conditions are imposed on the tangential field components. Additionally, the condition of local power finiteness and the radiation condition are to be satisfied. As the LEP is a source-free problem, we look for two real numbers, $\kappa=ka$ and γ, as eigenvalues [4] generating nonzero functions U. The first of these numbers is the normalized lasing frequency, while the second is the threshold material gain. Thanks to the real-valued k, the radiation condition at $r\to\infty$ is the usual 2-D Sommerfeld condition, so that the modal field does not diverge at infinity. Further we expand the field function inside each domain as

$$U(r,\varphi)=\sum_{m=0}^{\infty}[A_m^s J_m(kv_s r)+B_m^s H_m(kv_s r)]\cos m\varphi, \quad (1)$$

where $J_m(.)$ and $H_m^{(1)}(.)$ are the Bessel and Hankel functions, $s=1,\ldots,M$ is the number of the radial domain counted from the center, and M is the total number of contours (here $M=3$). From the condition of local energy finiteness and the radiation condition it follows that $B_m^1=0$ and $A_m^{M+1}=0$, respectively. Thanks to the circular symmetry, each term in Eq. (1) can be studied separately. Indeed, substitution of Eq. (1) into the boundary conditions associated with the sth boundary leads to the following two equations, valid independently for each value of the modal azimuth index $m=0,1,2,\ldots$:

$$\begin{aligned}&A_m^{s+1}J_m(\kappa v_{s+1}\rho_s)+B_m^{s+1}H_m^{(1)}(\kappa v_{s+1}\rho_s)\\&\quad=A_m^s J_m(\kappa v_s\rho_s)+B_m^s H_m^{(1)}(\kappa v_s\rho_s),\\&[A_m^{s+1}J_m'(\kappa v_{s+1}\rho_s)+B_m^{s+1}H_m^{(1)'}(\kappa v_{s+1}\rho_s)]/v_{s+1}\\&\quad=[A_m^s J_m'(\kappa v_s\rho_s)+B_m^s H_m^{(1)'}(\kappa v_s\rho_s)]/v_s,\end{aligned} \quad (2)$$

where $\rho_1=1$, $\rho_{s>1}=a_{s>1}/a$ are the normalized rim radii; $a_2=a+d$; $a_3=a_2+w$; $\nu_1=\nu=\alpha_a-\mathrm{Im}\,\gamma$; $\nu_{2,3}=\alpha_{g,r}$; and the prime denotes differentiation with respect to the argument. Collecting the equations like Eq. (2) from all boundaries, we obtain a $2M\times 2M$ matrix equation. In operator notation it can be written as $C^{(m)}X^{(m)}=0$, where $X^{(m)}=\{A_m^s,B_m^s\}_{s=1}^M$, and $C^{(m)}=\{C_{ij}^{(m)}\}_{i,j=1}^{2M}$ is a matrix operator. Then the search for the LEP eigenvalues reduces to finding the zeros of the infinite number of independent finite-order determinants,

$$\mathrm{Det}[C^{(m)}(\kappa,\gamma)]=0, \quad m=0,1,2,\ldots. \quad (3)$$

As suggested by the theory of functions of complex variables, the lasing-problem eigenvalues of each mth family form a discrete (i.e., infinite but countable) set on the plane (κ,γ). Thus, one angular index m is not enough to distinguish modes from each other, and another, radial, index must be used. To find eigenvalues, we use an in-house numerical algorithm based on the two-parameter secant-type iterative method, with initial guess values taken as the eigenvalues of κ and γ for the lasing modes in a stand-alone circular resonator—see [4]. This appears to be a more direct characterization of eigenvalues than looking for the values of κ and γ minimizing the amplitude of (in fact, nonexistent) in-going cylindrical waves in the host space, as was done in [16] within the transfer-matrix formalism.

3. EFFECT OF CONCENTRIC COUPLING

The characteristic equations derived are valid for arbitrary geometrical and material parameters. In our numerical study we assume that the microdisk and the ring are separated by the air gap, i.e., $\alpha_g=1$, and their pump-off refractive indices are the same, i.e., $\alpha_a=\alpha_r=2.63$. This value accords, for example, with the effective refractive index α_{eff}^H of the lowest *quasi*-TE-polarized mode in the air-clad GaAs/InP material systems for $\lambda=1.55$ μm, if the disk and ring thicknesses are 100 nm. In the same disk, the lowest quasi-TM-polarized modes have a much smaller effective refractive index, namely, $\alpha_{eff}^E=1.31$. Therefore they have much higher thresholds and can be ignored [4].

In Figs. 2(a) and 2(b), we present the dependences of the lasing frequencies and thresholds on the normalized disk-to-ring separation d/a for the dipole-type modes $H_{m,n,q,p}$ with $m=1$ in the cavity and with thin ring $w=0.2a$. Here, the first index m shows the number of the field variations in azimuth. The other indices, i.e., n, q, and, p, are the numbers of field variations in the active disk, air gap, and ring, respectively. In contrast to a single-disk cavity, here we have to keep several radial indices indicating mode field variations in each partial region. This is a reflection of the fundamental observation that the natural modes of the cavity made of several partial domains are in fact the "supermodes," i.e., combinations of optically coupled modes of separate domains. This situation is quite similar to that of the modes in a cavity built as a linear or cyclic photonic molecule [7–9].

At small values of d (the smallest value is $0.01a$ as indicated), the four modes in Figs. 2(a) and 2(b) denoted by the in-circle numbers 1 to 4 are the dipole modes with corresponding radial indices $n=1,2,3,4$, respectively, of the circular cavity of radius $a+w$ with an active central circle of radius a. This is highlighted by the dashed horizontal straight lines presenting the threshold and frequency values of the modes $H_{1,n}$ $(n=1,2,3,4)$ in the stand-alone active microdisk of radius a and material α_a [4]. As one can see, if the air-gap separation d is increased their lasing frequencies $\kappa_{1,n,q,p}$ decrease monotonically [Fig. 2(a)] and tend to the same value corresponding to the mode $H_{1,1}$ in the stand-alone disk of radius $a+w$ with active central circle of radius a (given by the horizontal dotted line). The threshold variation that accompanies the same change of

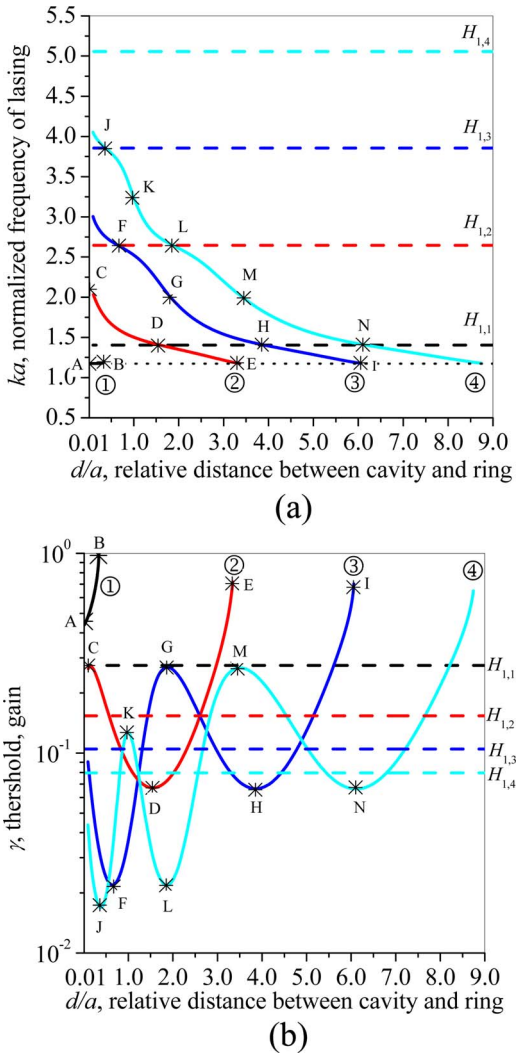

Fig. 2. (Color online) Normalized lasing frequencies (a) and thresholds (b) of the $H_{1,n,q,p}$ supermodes in the active disk loaded with a passive external dielectric ring versus the normalized air-gap separation between the disk and the ring. Ring thickness is $w=0.2a$, refractive indices are $\alpha_a=\alpha_r=2.63$, $\alpha_g=1$.

separation is more dramatic (by several times) both in the sense of reduction and growth [Fig. 2(b)]. Broadly speaking, at any specific value of d/a there are two or three modes whose frequencies are near the mentioned limiting value. The one whose frequency is nearer to the frequency of the $H_{1,1}$ mode in the stand-alone all-active disk of radius a, $\kappa_{1,1}=1.405$, always has the smallest threshold.

The locations of the minima and maxima and their extreme values correlate with the transformation of the mode patterns along the structure radius—see Fig. 3 for the H-field patterns visualized at the points marked in Fig. 2(a). The minima of thresholds are observed if high-intensity H-field spots concentrate in the active region, and the leakage out of the cavity is reduced (Figs. 3 D, F, H, J, L, N). The maxima of thresholds appear in the situations when intensive field spots are pushed out of the active region to the air gap between the cavity and the ring (Figs. 3 C, E, G, I, K, M). This is accompanied by increased leakage. Moving the ring away from the active cavity leads to the field redistribution inside the structure that can be characterized by the varying partial indices n and q. Note that for the modes presented in Figs. 2 and 3, the passive ring thickness is fixed and has the small value $w=0.2a$ so that the "ring" index $p=0$.

It is interesting to note that if d/a changes, all eigenvalues of the considered $H_{1,n,q,0}$ supermodes migrate along one and the same trajectory on the plane (κ,γ). Increasing the distance from the disk to the ring just moves the eigenvalues along this trajectory from the right to the left as shown in Fig. 4. However, the start point on this trajectory is different for each dipole-type supermode. These start points are marked with open symbols in Fig. 4 and correspond to the modes $H_{1,n}$ in the stand-alone disk of radius $a+w$ with active central circle of radius a. Therefore, such a trajectory on the plane (κ,γ) seems to be a sort of signature for the dipole-mode family $(m=1)$. Its shape, however, depends on the radii and material composition of the ringlike passive domains.

A different type of the mode behavior is observed if we change the passive ring thickness while the air-gap thickness is fixed. The dependences of the lasing frequencies and thresholds on the normalized ring thickness w/a are presented in Fig. 5. The frequency dependences are piecewise monotonic [Fig. 5(a)], with each monotonic section corresponding to the different mode type in terms of the "ring" partial radial index p. This is revealed after visualization of the corresponding H-field patterns at the marked points (see Fig. 6). Here, all near-field patterns labeled from B to K demonstrate high confinement of the optical field in the central active disk, while the pattern labeled A shows considerable leakage out of the cavity. Indeed the latter pattern corresponds to threshold near a local maximum in Fig. 5, and the patterns from B to K have been computed in the minima of thresholds. Varying the ring thickness results in the appearance of new H-field variations in the ring while the numbers of variations in the cavity and air gap, n and q, are the same. On the plots of modal thresholds as a function of w/a in Fig. 5(b), one can see again a series of minima and maxima of the thresholds. The minima occur at the middle points of the monotonic frequency-dependence sections, and the threshold maxima correspond to their "ends," where the modes transform from one type to another, with the partial "ring" index p changing by one.

4. OPTICAL THEOREM FOR THE LASING MODES

The plots of mode thresholds versus the cavity parameters and the mode H-field patterns show a certain correlation that calls for an accurate quantification. Fortunately, a tool for such quantification already exists in the theory of Maxwell's equations—this is the optical theorem (OT). The OT is the real-valued identity that is derived from the complex-valued Poynting theorem [19] in the time-harmonic plane wave scattering and links the total extinction cross section of a scatterer with the amplitude of the forward-scattered field in the far zone. The Poynting theorem can also be applied to any field functions satisfying Maxwell's equations in the absence of given currents or incident field, i.e., to the eigensolutions. The most general form of the resulting identity, for the complex-valued k, is

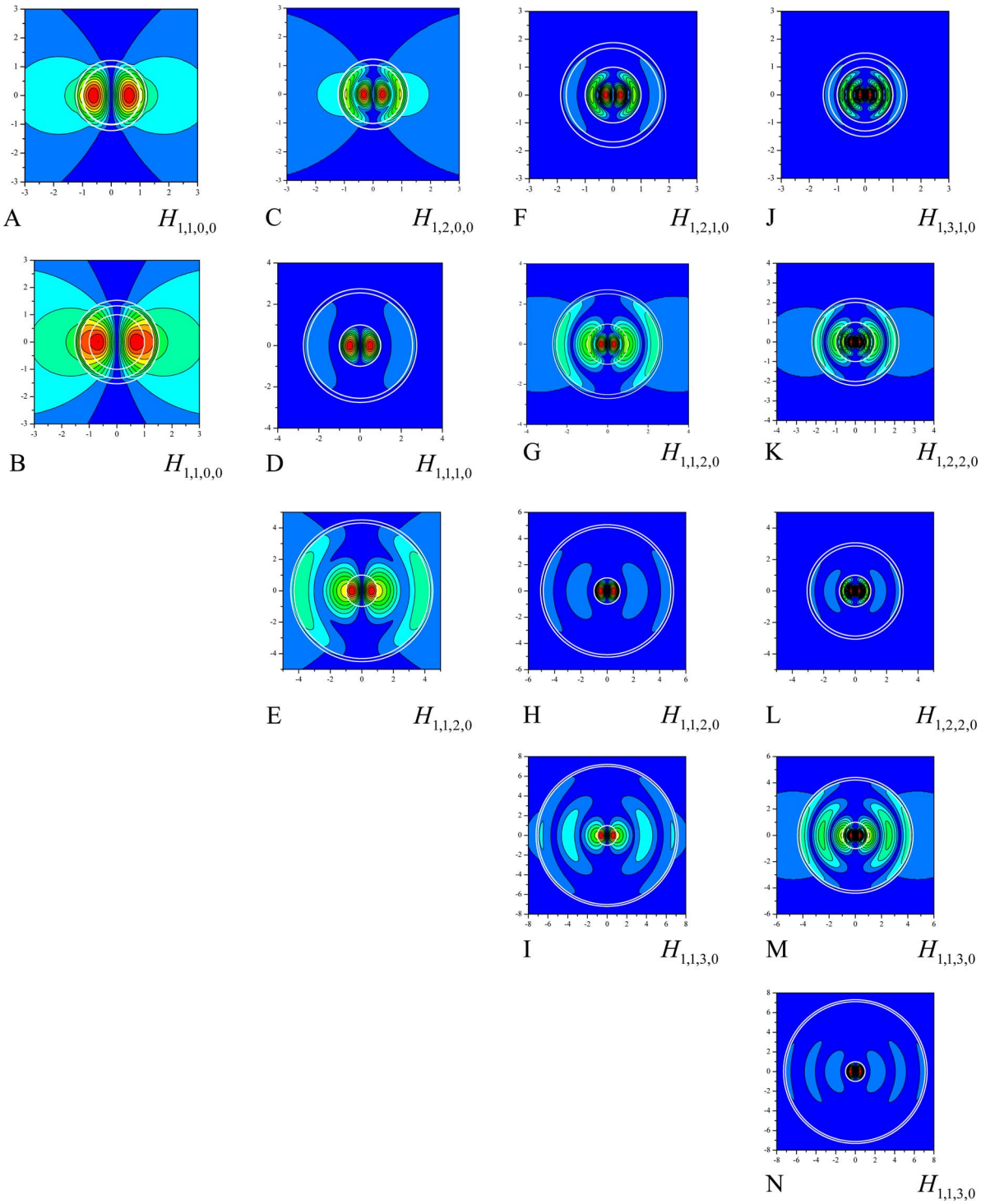

Fig. 3. (Color online) Near-field $|H_z(r,\varphi)|$ patterns for the supermodes $H_{1,n,q,p}$ at the points marked in Fig. 2; ring thickness is $w=0.2a$, refractive indices are $\alpha_a=\alpha_r=2.63$, $\alpha_g=1$.

$$\left(\frac{1}{2}\right)\oint_S \vec{E}\times\vec{H}^*\mathrm{d}s = (i/2)\int_V (k^*\varepsilon^* Z_0^{-1}|\vec{E}|^2 - k\mu Z_0|\vec{H}|^2)\mathrm{d}v, \tag{4}$$

where the left-hand part is the total outward flux of the Poynting vector averaged over the period of oscillations through the boundary S of the "minimum sphere" V containing all passive and active regions (so that the domain outside it is homogeneous and filled with air); piecewise continuous functions ε and μ are the relative permittivity and permeability, respectively; and the asterisk means complex conjugation.

Suppose now that we are considering a generic lasing mode, to which we will assign, for brevity and in view of discreteness of the LEP eigenvalues, a single cumulative

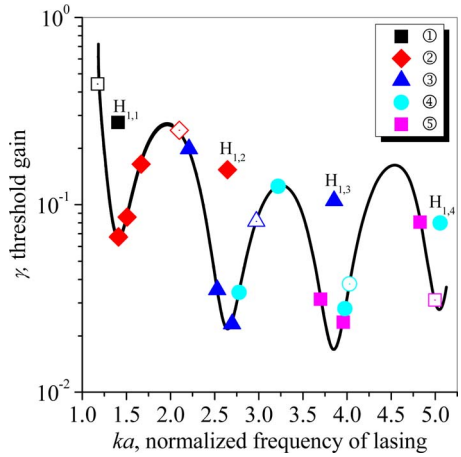

Fig. 4. (Color online) Eigenvalue migration on the plane (κ,γ) when the air-gap separation parameter d/a varies. Ring thickness is $w=0.2a$, refractive indices are $\alpha_a=\alpha_r=2.63$, $\alpha_g=1$. In-circle numbers correspond to the mode notations of Fig. 2. The open symbols correspond to eigenvalues for supermodes $H_{1,n,q,p}$ at the initial value of the parameter $d/a=0.01$. The filled color symbols on the curve correspond to eigenvalues of supermodes $H_{1,n,q,p}$ at $d/a=0.5$, 1.0, 1.5 (from right to left). The off-curve symbols correspond to the eigenvalues for the all-active disk of radius a.

index j. We apply Eq. (4) to the corresponding mode field $\{\vec{E}_j,\vec{H}_j\}$, taking into account that $\mathrm{Im}\,k_j=0$ and the active-region dielectric constant is $\varepsilon_a=\nu_j^2=\alpha^2-\gamma_j^2-2i\alpha\gamma_j$, and additionally assuming that all materials are nonmagnetic, $\mu=1$. Then the OT tells that, for the lasing mode number j, the radiation losses are exactly balanced with the power generated in the active region V_a, provided that the material gain equals γ_j:

$$(Z_0/2)\mathrm{Re}\oint_S \vec{E}_j\times\vec{H}_j^*\mathrm{d}s=\gamma_j k_j\alpha_a\int_{V_a}|\vec{E}_j(\vec{R},k_j,\gamma_j)|^2\mathrm{d}v, \quad (5)$$

where $\vec{R}$ is a radius vector.

In the case of the laser depicted in Fig. 1, the active region is only a part of the whole cavity volume, which also contains the air gap V_g and the ring V_r. Therefore it is convenient to introduce, for each jth mode, the total mode volume,

$$W_j(k_j,\gamma_j)=\int_V \alpha_a^2|\vec{E}_j(\vec{R},k_j,\gamma_j)|^2\mathrm{d}v=\int_{V_a}\alpha_a^2|\vec{E}_j|^2\mathrm{d}v+\int_{V_g}\alpha_g^2|\vec{E}_j|^2\mathrm{d}v+\int_{V_r}\alpha_r^2|\vec{E}_j|^2\mathrm{d}v, \quad (6)$$

and also the partial factors $\Gamma_j^{(a)},\Gamma_j^{(g)},\Gamma_j^{(r)}\leqslant 1$:

$$\Gamma_j^{(f)}=W_j^{(f)}/W_j,\quad W_j^{(f)}(k_j,\gamma_j)=\int_{V_f}\alpha_f^2|\vec{E}_j(\vec{R},k_j,\gamma_j)|^2\mathrm{d}v,\quad f=a,g,r. \quad (7)$$

The meaning of each factor is a measure of the overlap of the corresponding active or passive region with the E-field of the jth mode; note that $\Gamma_j^{(a)}+\Gamma_j^{(g)}+\Gamma_j^{(r)}=1$. It is important to remember that these quantities make sense

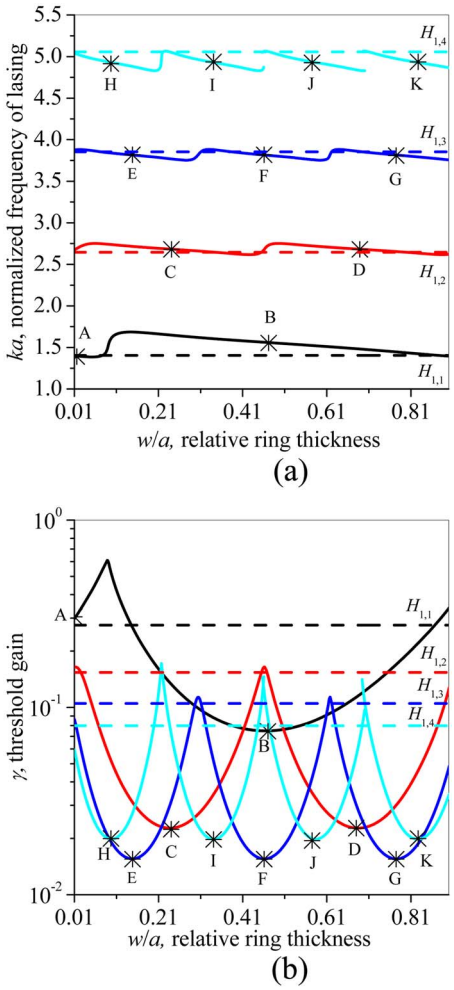

Fig. 5. (Color online) Normalized lasing frequencies (a) and thresholds (b) of the $H_{1,n,q,p}$ modes in the active disk placed inside a passive ring versus the normalized ring thickness. Air-gap separation is $d=0.5a$, and refractive indices are $\alpha_a=\alpha_r=2.63$, $\alpha_g=1$.

only as discrete values linked to the modes. Now the OT given by Eq. (5) can be rewritten as

$$\gamma_j=\frac{(Z_0/2)\mathrm{Re}\oint_S \vec{E}_j\times\vec{H}_j^*\mathrm{d}s}{k_j\alpha_a\int_{V_a}|\vec{E}_j(\vec{R},k_j,\gamma_j)|^2\mathrm{d}v}=\frac{\alpha_a P_j}{\Gamma_j^{(a)}k_j W_j}, \quad (8)$$

where

$$P_j=(Z_0/2)\mathrm{Re}\oint_S \vec{E}_j\times\vec{H}_j^*\mathrm{d}s \quad (9)$$

is the flux of power lost for radiation or the emission cross section. All quantities in the right-hand part of Eq. (8) are determined by the integration of the field functions, which indirectly depend on the material gain γ_j through the Maxwell equations. The quantity P_j/k_jW_j is the ratio of the radiated powers to the powers stored inside the whole cavity, thus its inverse has the meaning of the "Q factor" of the cavity with active region $\tilde{Q}_j$, and hence

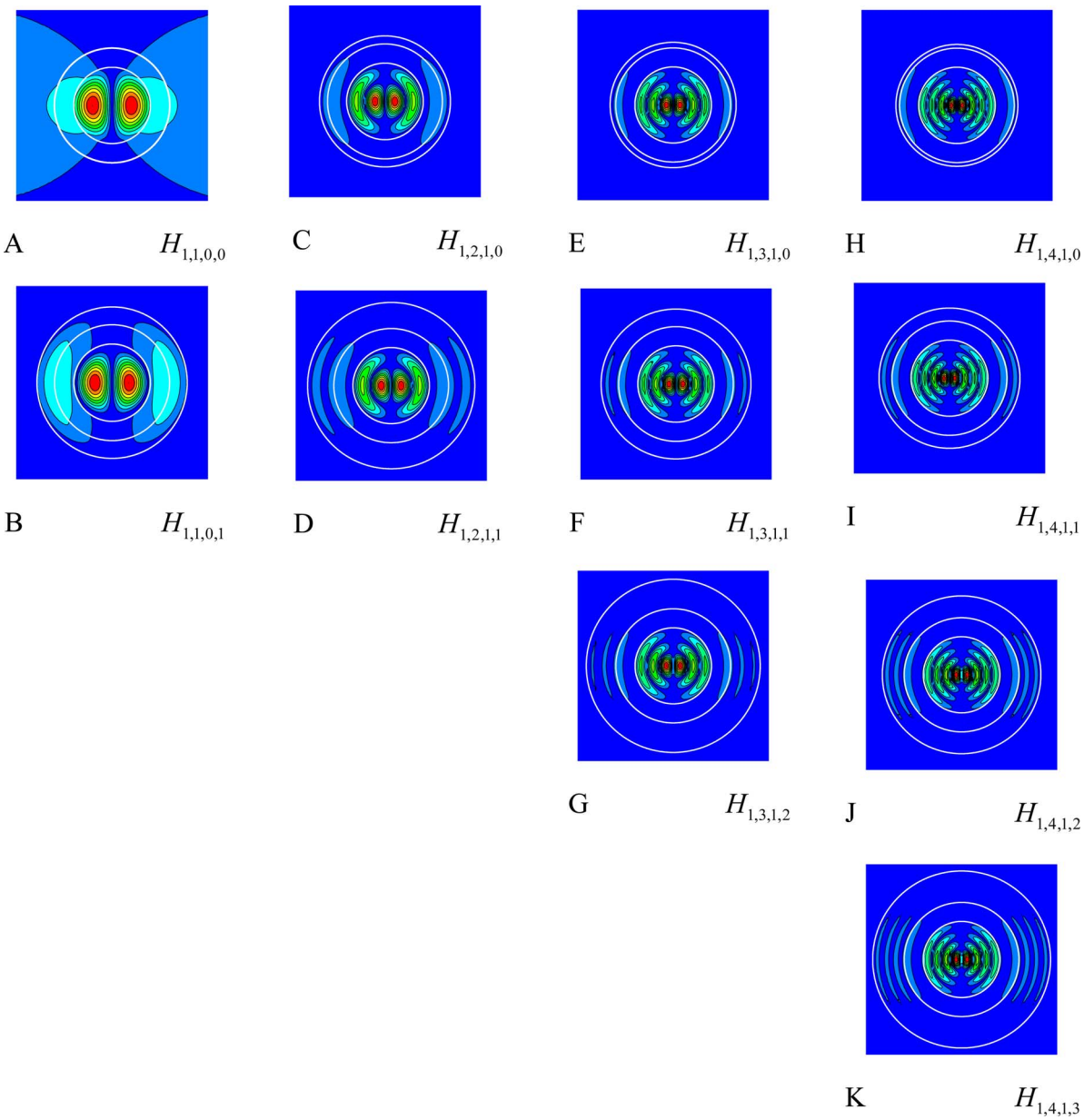

Fig. 6. (Color online) Near-field $|H_z(r,\varphi)|$ patterns for the supermodes $H_{1,n,q,p}$ at the minima of threshold γ corresponding to the points marked by B to K in Fig. 5. Conversely, case A corresponds to the high threshold. Air-gap separation is $d=0.5a$, refractive indices are $\alpha_a=\alpha_r=2.63$, $\alpha_g=1$.

$$\gamma_j=\frac{\alpha_a}{\Gamma_j^{(a)}\tilde{Q}_j}. \tag{10}$$

This simple formula is very insightful. Indeed, as both $\Gamma_j^{(a)}$ and $\tilde{Q}_j$ depend on the squared field components, their changes with respect to small variations in the threshold $\delta\gamma$ are $\Delta=O[(\delta\gamma)^2]$. Therefore if $\gamma_j\ll 1$ then, in the first approximation, one may take both $\Gamma_j^{(a)}$ and $\tilde{Q}_j$ as the values calculated by neglecting γ_j. It means that one may take the passive cavity Q factor, $Q_j=\mathrm{Re}\,k_j/2|\mathrm{Im}\,k_j|$, as the approximate substitute for $\tilde{Q}_j$ and calculate the active-region mode overlap factor by using the passive-cavity field functions.

Thus, a high Q factor in the pump-off regime is not enough for the low threshold in the pump-on case, because it can be spoiled by the poor overlap between the mode electric field and the active region. In the simplest case of a fully active cavity (this can be only a free-standing slab in 1-D, a circle in 2-D, and a sphere in 3-D), $\Gamma_p^{(a)}\equiv 1$ and $\gamma_j=\alpha_a/\tilde{Q}_j\approx\alpha_a/Q_j$.

5. NUMERICAL ANALYSIS WITH THE AID OF OVERLAP FACTORS

In our laser consisting of the concentrically coupled active disk and passive ring, the computation of the overlap factors for the TE modes leads to the necessity of integrating the squares and cross products of cylindrical functions and their derivatives of the same index m (mode angular index). In each partial domain, the expressions resulting

from Eq. (1) lead to the following generic-form integrals (here we omit the domain index f and the argument of cylindrical functions $\kappa\nu_f\rho$):

$$W_s = \int_{V_s} \alpha^2|E|^2\rho\mathrm{d}\rho\mathrm{d}\varphi$$
$$= \frac{\pi\alpha^2 Z_0^2}{2\nu_s\nu_s^*}\int_{a_s}^{a_{s+1}} [|A_m^s|^2(J_{m-1}J_{m-1}^* + J_{m+1}J_{m+1}^*)$$
$$+ A_m^s B_m^{s*}(J_{m-1}H_{m-1}^{(1)*} + J_{m+1}H_{m+1}^{(1)*}) + A_m^{s*}B_m^s(J_{m-1}^*H_{m-1}^{(1)}$$
$$+ J_{m+1}^*H_{m+1}^{(1)})$$
$$+ |B_m^s|^2(H_{m-1}^{(1)}H_{m-1}^{(1)*} + H_{m+1}^{(1)}H_{m+1}^{(1)*})]\rho\mathrm{d}\rho. \quad (11)$$

Depending on whether we have an active domain or a passive one, this involves the products of functions with either complex-conjugate arguments or the same real-valued argument. Correspondingly we have to apply one of two explicit formulas, one found in [20],

$$\int Z_m(\kappa\nu\rho)T_m(\kappa\nu^*\rho)\rho\mathrm{d}\rho$$
$$= \frac{\rho}{\kappa}\left[\frac{\nu^* Z_m(\kappa\nu\rho)T_{m-1}^*(\kappa\nu\rho) - \nu_j Z_{m-1}^*(\kappa\nu\rho)T_m(\kappa\nu\rho)}{\nu^2 - \nu^{*2}}\right], \quad (12)$$

and the other obtained from Eq. (12) with the aid of some algebra in the limiting case as $\mathrm{Im}\,\nu \to 0$,

$$\int Z_m(\kappa\alpha\rho)T_m(\kappa\alpha\rho)\rho\mathrm{d}\rho = \frac{\rho^2}{4}[2Z_m(\kappa\alpha\rho)T_m(\kappa\alpha\rho)$$
$$- Z_{m-1}(\kappa\alpha\rho)T_{m+1}(\kappa\alpha\rho)$$
$$- Z_{m+1}(\kappa\alpha\rho)T_{m-1}(\kappa\alpha\rho)], \quad (13)$$

where $Z_m(\cdot)$ and $T_m(\cdot)$ are arbitrary cylindrical functions.

Note that the analog of Eq. (13) given as Eq. (B3) of Appendix B of [14] is wrong because of the lost "2" before the first term and the extra "2" before the second and third terms. Indeed, if in Eq. (B3) one changes the Neumann function to the Bessel function one must obtain formula (B3). However, the mistakes in the coefficients noted prevent it.

Using formula (12) we find that the electric field power stored in the central active circle is

$$W_{mn}^{(a)} = \frac{Z_0^2 A_0^2 a^2}{2\gamma_{mn}\kappa_{mn}}\,\mathrm{Im}[\nu_{mn}J_m(\kappa\nu_{mn}^*)J_{m-1}(\kappa\nu_{mn})]. \quad (14)$$

. The electric field power contained in a passive ringlike domain is computed according to Eq. (11) that involves 16 terms generated by Eq. (13) with corresponding limits of integration.

The plots in Fig. 7 demonstrate the dynamics of the $H_{1,n,q,p}$ mode overlap coefficients for three regions of the considered laser cavity (active circle, passive air-gap ring, and passive dielectric ring) as a function of the relative size of the air gap, i.e., they correspond to the plots in Fig. 2. As one can observe, the air-gap overlap coefficients $\Gamma_{1,n,q,p}^{(g)}$ behave very similarly to the mode thresholds $\gamma_{1,n,q,p}$ [see Fig. 2(b)], while the active-region overlap coefficients $\Gamma_{1,n,q,p}^{(a)}$ behave similarly to the inverse values of the thresholds. This is because here the dielectric-ring thickness is small ($w = 0.2a$) and, as a result, the ring overlap coefficients are a small fraction of unity unless the ring shrinks to the active region—see Fig. 7(c). Thus, low-threshold regimes correspond to the mode E field being pulled into the active region, while the high thresholds correspond to the field being pushed out of it, i.e., into

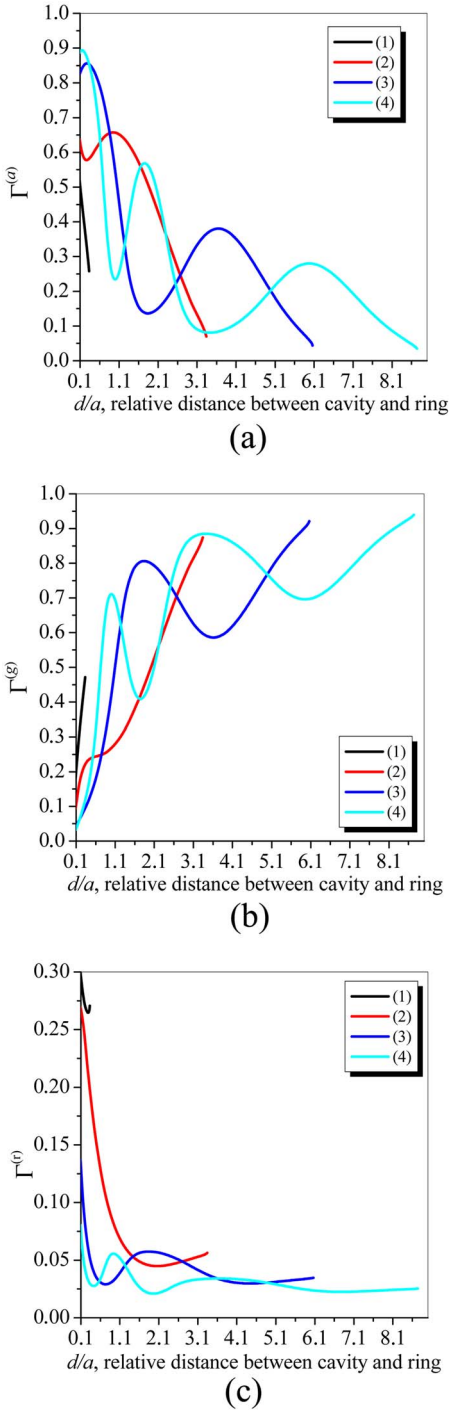

Fig. 7. (Color online) Active-region (a), passive air-gap (b), and passive ring (c) mode overlap factors for the $H_{1,n,q,p}$ supermodes in the active disk loaded with a passive dielectric ring versus the normalized air-gap separation between the disk and the ring. Other parameters are the same as in Fig. 2.

the air gap in the case of the narrow ring. If the dielectric ring gets wider, then the E field can be effectively pulled into the ring as well. Therefore the threshold variations in Fig. 5 are explained by the E field's redistribution between the active region, the air gap, and the ring. Sharp jumps in thresholds are always caused by the formation of new electric field variations (additional bright spots) in the ring, i.e., changing the "ring" partial index p by one. All these variations occur in full agreement with expression (10).

6. CONCLUSIONS

We have studied numerically the lasing frequencies and thresholds for the non-WG dipole-type modes in a 2-D model of an active microdisk enclosed by a concentric passive microring. A specialized linear eigenvalue problem, i.e., the LEP, has enabled our doing this in a mathematically flawless and physically transparent manner. We have demonstrated that the mode thresholds can be lowered by an order with respect to the corresponding values in a stand-alone disk, provided that the separation between the active cavity and the ring and the thickness of the latter are tuned properly. However, because of the presence of the ring, the dipole mode of the active disk splits into a multiplet of the supermodes, each of them having a certain number of field variations in radius along the whole combined structure. This is clearly revealed by the near-field mode patterns. If the air-gap size varies, the supermode eigenparameters move along the same trajectory on the frequency-threshold plane, in turn demonstrating a similar threshold reduction when the frequency approaches one of the values corresponding to the $H_{1,n}$ modes in the stand-alone active cavity.

Trying to understand the thresholds' behavior in such a wavelength-scale combined optical cavity, we have come to the necessity of studying the partial-region overlap coefficients with the mode E-field pattern. These quantities for the active and passive parts of the cavity are suggested by the classical OT applied to the lasing-mode field. Their computation has shown that it is the active-region overlap coefficient that always correlates with the inverse value of the threshold for a given mode.

It is expected that the results obtained can shed new light on the complicated mode behavior in ABR-assisted microdisk lasers having larger numbers of partial passive regions (rings and grooves) optically coupled with the central active region whose low-index mode threshold the ABR is hoped to reduce.

ACKNOWLEDGMENTS

This work was supported in part by the National Academy of Sciences of Ukraine (NASU) via project 07/36-H; the Royal Society, UK, via project IJP-2007/R1-FS; and the Academy of Sciences of the Czech Republic (ASCR), jointly with NASU, via an exchange program. The first author was also supported by the International Visegrad Fund with a Ph.D. scholarship.

REFERENCES AND NOTES

1. A. B. Matsko and V. S. Ilchenko, "Optical resonators with whispering-gallery modes-part 1: basics," IEEE J. Sel. Top. Quantum Electron. **12**, 3–14 (2006).
2. V. S. Ilchenko and A. B. Matsko, "Optical resonators with whispering-gallery modes-part 2: applications," IEEE J. Sel. Top. Quantum Electron. **12**, 15–32 (2006).
3. A. I. Nosich, E. I. Smotrova, S. V. Boriskina, T. M. Benson, and P. Sewell, "Trends in microdisk laser research and linear optical modeling," Opt. Quantum Electron. **39**, 1253–1272 (2007).
4. E. I. Smotrova, A. I. Nosich, T. Benson, and P. Sewell, "Cold-cavity thresholds of microdisks with uniform and non-uniform gain: quasi-3D modeling with accurate 2D analysis," IEEE J. Sel. Top. Quantum Electron. **11**, 1135–1142 (2005).
5. P. W. Evans and N. Holonyak, Jr., "Room temperature photopump laser operation of native-oxide-defined coupled GaAs-AlAs superlattice microrings," Appl. Phys. Lett. **69**, 2391–2393 (1996).
6. A. Nakagawa, S. Ishii, and T. Baba, "Photonic molecule laser composed of GaInAsP microdisks," Appl. Phys. Lett. **86**, 041112 (2005).
7. S. V. Boriskina, "Theoretical prediction of a dramatic Q-factor enhancement and degeneracy removal of WG modes in symmetrical photonic molecules," Opt. Lett. **31**, 338–340 (2006).
8. E. I. Smotrova, A. I. Nosich, T. M. Benson, and P. Sewell, "Optical coupling of WG modes in two identical microdisks and its effect on the lasing spectra and thresholds," IEEE J. Sel. Top. Quantum Electron. **12**, 78–85 (2006).
9. E. I. Smotrova, A. I. Nosich, T. M. Benson, and P. Sewell, "Threshold reduction in a cyclic photonic molecule laser composed of identical microdisks with WG modes," Opt. Lett. **31**, 921–923 (2006).
10. E. I. Smotrova, A. I. Nosich, T. M. Benson, and P. Sewell, "Ultralow lasing thresholds of the pi-type supermodes in cyclic photonic molecules composed of sub-micron disks with monopole and dipole modes," IEEE Photon. Technol. Lett. **18**, 1993–1995 (2006).
11. A. Jebali, R. F. Mahrt, N. Moll, C. Bauer, G. L. Bona, and W. Bachtold, "Lasing in organic circular grating structures," J. Appl. Phys. **96**, 3043–3049 (2004).
12. D. Labilloy, H. Benisty, and C. Weisbuch, "High-finesse disk microcavity based on a circular Bragg reflector," Appl. Phys. Lett. **73**, 1314–1316 (1998).
13. M. Born and E. Wolf, *Principles of Optics*, 4th ed., (Pergamon, 1968).
14. A. Jebali, D. Erni, S. Gulde, R. F. Mahrt, and W. Bachtold, "Analytical calculation of the Q factor for circular-grating microcavities," J. Opt. Soc. Am. B **24**, 906–915 (2007). Note that the radiation power loss is found from a formulation implying that a unit source is located at the origin [see Eq. (14)], while the stored power is found from a standing-wave source-free formulation [see Eq. (22)]. These are two different electromagnetic problems, so it is erroneous to blend their solutions together in the calculation of Q factor.
15. X. Sun and A. Yariv, "Modal properties and modal control in vertically emitting annular Bragg lasers," Opt. Express **15**, 17323–17333 (2007).
16. J. Scheuer, "Radial Bragg lasers: optimal design for minimal threshold levels and enhanced mode discrimination," J. Opt. Soc. Am. B **24**, 2178–2184 (2007).
17. H.-J. Moon, G.-W. Park, S.-B. Lee, K. An, and J.-H. Lee, "Laser oscillations of resonance modes in a thin gain-doped ring-type cylindrical microcavity," Opt. Commun. **235**, 401–406 (2004).
18. Z. Zhang, L. Yang, V. Liu, T. Hong, K. Vahala, and A. Scherer, "Visible submicron microdisk lasers," Appl. Phys. Lett. **90**, 111119 (2007).
19. G. Hanson and A. Yakovlev, *Operator Theory for Electromagnetics* (Springer-Verlag, 2002).
20. I. S. Gradshteyn and I. M. Ryzhik, *Table of Integrals, Series, and Products* (Academic, 1980).